Downloaded from rnajournal.cshlp.org on January 20, 2020 - Published by Cold Spring Harbor Laboratory Press

"End-to-end" stacking of small dsRNA

NICOLE ERLENBACH,[1] CHRISTIAN GRÜNEWALD,[2] BISERA KRSTIC,[1] ALEXANDER HECKEL,[2] and THOMAS F. PRISNER[1]

[1]Institute of Physical and Theoretical Chemistry, Center of Biomolecular Magnetic Resonance, Goethe University, D-60438 Frankfurt am Main, Germany

[2]Institute of Organic Chemistry and Chemical Biology, Goethe University, D-60438 Frankfurt am Main, Germany

ABSTRACT

PELDOR (pulsed electron–electron double resonance) is an established method to study intramolecular distances and can give evidence for conformational changes and flexibilities. However, it can also be used to study intermolecular interactions as for example oligerimization. Here, we used PELDOR to study the "end-to-end" stacking of small double-stranded (ds) RNAs. For this study, the dsRNA molecules were only singly labeled with the spin label TPA to avoid multispin effects and to measure only the intermolecular stacking interactions. It can be shown that small dsRNAs tend to assemble to rod-like structures due to π–π interactions between the base pairs at the end of the strands. On the one hand, these interactions can influence or complicate measurements aimed at the determining of the structure and dynamics of the dsRNA molecule itself. On the other hand, it can be interesting to study such intermolecular stacking interactions in more detail, as for example their dependence on ion concentration. We quantitatively determined the stacking probability as a function of the monovalent NaCl salt and the dsRNA concentration. From these data, the dissociation constant K_d was deduced and found to depend on the ratio between the NaCl salt and dsRNA concentrations. Additionally, the distances and distance distributions obtained predict a model for the stacking geometry of dsRNAs. Introducing a nucleotide overhangs at one end of the dsRNA molecule restricts the stacking to the other end, leading only to dimer formations. Introducing such an overhang at both ends of the dsRNA molecule fully suppresses stacking, as we demonstrate by PELDOR experiments quantitatively.

Keywords: EPR; PELDOR/DEER; dsRNA; stacking

INTRODUCTION

In 1958 it was recognized that the hydrogen bonds between the complementary base pairs in double-stranded nucleic acids (dsNA) (Fonseca Guerra et al. 1999) cannot be the only interaction stabilizing the secondary structure of duplexes (Sturtevant et al. 1958). An additional effect of parallel aromatic stacking by London dispersion forces between the base pairs above and below each other was found, also known as π–π interaction (van de Waal 1986; Mignon et al. 2005). This intramolecular interaction was studied intensively in the last decade using experimental and computational methods (Hunter and Sanders 1990; Gellman et al. 1996; Florián et al. 1999; Brown et al. 2015; Häse and Zacharias 2016; Kilchherr et al. 2016; Šponer et al. 2018). However, this inter-residue interaction is not only an intramolecular effect; it can also be observed as intermolecular interaction between two duplexes. In such cases, the short dsNAs stack spontaneously into rod-like structures, which were first observed for DNA in liquid crystals (Nakata et al. 2007). The "end-to-end" stacking was the only possible way to explain the axial ordering in these crystals. Previous studies had primarily focused on "side-by-side" forces between long dsDNA (Oosawa 1968; Allahyarov et al. 2004; Maffeo et al. 2010; Wong and Pollack 2010).

Rod-like stacking can play an important role in RNA–protein interactions, as shown by Ryter and Schulz (1998). They studied the interaction between a dsRNA-binding domain and two ten base pair long dsRNAs. These dsRNAs stacked with each other to form a pseudo-continuous helix. The stacking expanded the major groove, which seemed to create the binding site for the protein.

The Pollack group (Qiu et al. 2006; Pollack 2011) studied "end-to-end" stacking of dsDNA with small angle X-ray scattering (SAXS). They were able to differentiate between repulsion and attraction of two dsNA, and they studied the

Corresponding author: prisner@chemie.uni-frankfurt.de

Article is online at http://www.rnajournal.org/cgi/doi/10.1261/rna.068130.118.

© 2019 Erlenbach et al. This article is distributed exclusively by the *RNA* Society for the first 12 months after the full-issue publication date (see http://rnajournal.cshlp.org/site/misc/terms.xhtml). After 12 months, it is available under a Creative Commons License (Attribution-NonCommercial 4.0 International), as described at http://creativecommons.org/licenses/by-nc/4.0/.

Downloaded from rnajournal.cshlp.org on January 20, 2020 - Published by Cold Spring Harbor Laboratory Press

contribution of salt concentration, of DNA concentration and of the number of base pairs to the attraction and repulsion forces between short dsDNA (Qiu et al. 2007). In the case of dsRNA, they found that the nearby divalent Mg^{2+} ion distribution shields the negative charge of the nucleic acids more effectively compared to dsDNA. They also found that for dsRNAs the π–π attraction plays an important role even at low salt concentrations (Pabit et al. 2009).

Another method to study these interactions is electron paramagnetic resonance spectroscopy (EPR). Pulsed electron–electron double resonance spectroscopy (PELDOR/DEER) (Milov et al. 1984; Martin et al. 1998) is a method for measuring distances in a range of 2–10 nm (Fig. 1). However, paramagnetic reporter groups attached to the biomolecule are required for such measurements. Commonly used modified nucleic acids are aminoxyl radicals based spin labels, called nitroxides. The well-established spin-label 2,2,5,5-tetramethyl-pyrrolin-1-oxyl-3-acetylene (TPA, chemical structure depicted in Fig. 2A) is used for dsNA (Spaltenstein et al. 1989) and produces reliable distances (Schiemann et al. 2007). Such measurements were performed to obtain information about structure and about dynamic and conformational changes of different kinds of NAs (Krstić et al. 2010; Romainczyk et al. 2011). The experimental PELDOR time trace (Fig. 1C) can be described as a product of the specific intramolecular interaction between the two spin labels on the RNA molecule (giving rise to a well-defined oscillation) and the nonspecific intramolecular interaction between all molecules in the sample (resulting in an exponential decaying background function). After background division and normalization (to the signal intensity for $\Delta t = 0$) of the PELDOR time trace (Fig. 1D), Tikhonov regularization can be used to extract from the oscillations of the time trace the distance distribution function $P(r)$ between both spin labels (Fig. 1E).

However, the PELDOR method is not limited to intramolecular interactions. Wherever specific intermolecular distances in the 2–10 nm range appear, for example in oligomerization of membrane proteins (Endeward et al. 2009) or "end-to-end" stacking of RNA, these distances can be measured by this method. Such distances have already been observed in previously published PELDOR measurements of NAs (Piton et al. 2007; Romainczyk et al. 2011; Halbmair et al. 2016; Weinrich et al. 2017) and were especially pronounced for RNA molecules. Whereas only one distinct distance was expected for short dsRNAs with two spin labels, additional distances were observed. Compared with dsRNA models, it was clear that these additional distances could only be explained by "end-to-end" stacking between dsRNA molecules. However, a detailed analysis of the intramolecular distances is more difficult in such cases, because more than two coupled spins contribute to the PELDOR signal (Bode et al. 2007).

In addition to information on distances, a PELDOR time trace also provides information about the number of spins interacting within an ~10 nm sphere. The modulation depth Δ of the background corrected and normalized PELDOR signal (Fig. 1D) reports on the number of interacting spins. This was recognized by Milov et al. (1998) and used for spin counting in multispin molecules (Bode et al. 2007). However, this method is not only useful in determining the number of spins per macromolecule but also in assessing the stacking of singly spin-labeled dsRNA molecules. In this case, a direct correlation of the experimental easy accessible modulation depth Δ and the dsRNA stacking probability P exists, allowing a quantitative determination of the thermodynamic equilibrium between stacked and unstacked dsRNA molecules.

In this paper, we investigated the influence of the monovalent NaCl salt concentration and of dsRNA concentration itself on the stacking probability p. For this specific purpose, the dsRNAs were only mono-labeled with the TPA spin label. Hence, only intermolecular distances arising from stacking of the dsRNAs are visible in our PELDOR measurements. From the distance distribution functions $P(r)$ derived from the PELDOR time traces the end-to-end stacking geometry could be deduced. The influence of dsRNA concentration and of the salt concentration was studied by PELDOR spectroscopy. The stacking probability could be quantitatively determined from the modulation depth Δ, as a function of NaCl salt and dsRNA concentration. From this, the dissociation constant K_d of the stacking could be calculated. Additionally, we could demonstrate that stacking of short dsRNAs can be quantitatively avoided by

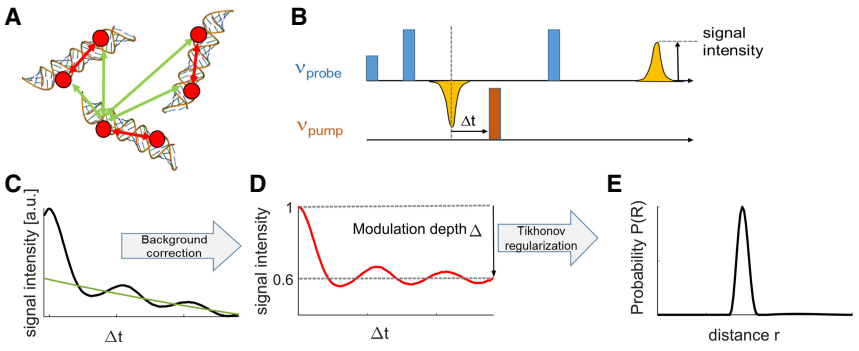

FIGURE 1. (*A*) Cartoon of possible intramolecular (red) and intermolecular (green) interactions in doubly labeled dsRNA molecules. (*B*) Four-pulse PELDOR sequence. (*C*) Raw PELDOR time trace (black) with intermolecular mono-exponential background (green). (*D*) Background corrected PELDOR time trace with only intramolecular interaction. The modulation depth Δ is indicated in the figure. (*E*) Distance distribution derived from a Tikhonov regularization of the background corrected PELDOR time traces.

Downloaded from rnajournal.cshlp.org on January 20, 2020 - Published by Cold Spring Harbor Laboratory Press

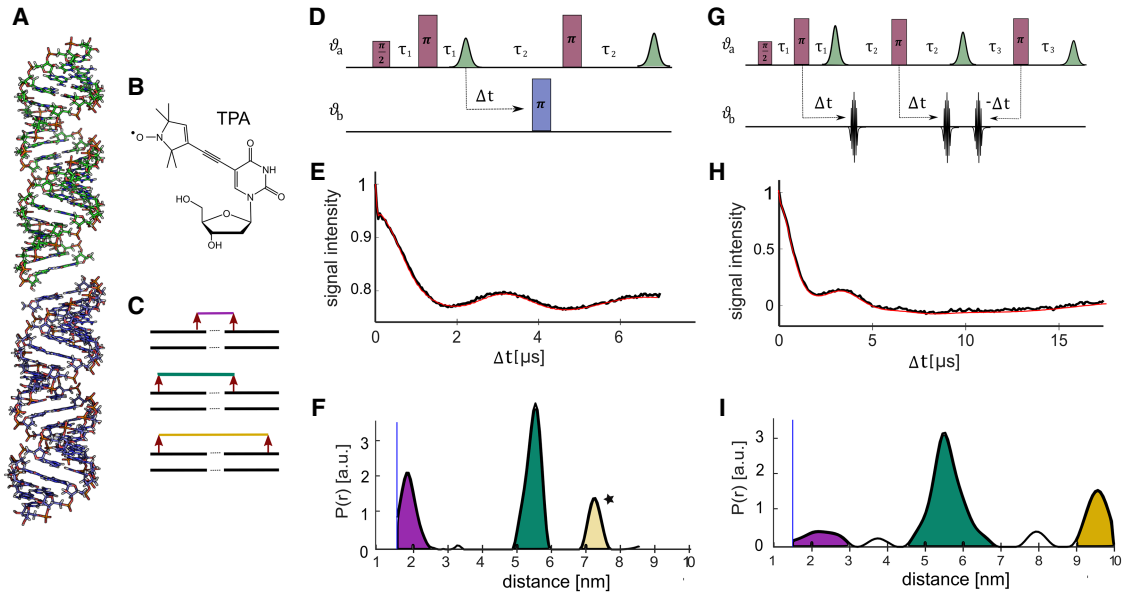

FIGURE 2. (*A*) Model of a stacked dsRNA dimer. (*B*) Chemical structure of TPA. (*C*) Three stacking possibilities, which relate to three different measurable distances in a singly labeled dsRNA sample. (*D*) Pulse sequence of the four-pulse PELDOR experiment. (*E*) Background corrected four-pulse PELDOR time trace for a stacked singly labeled dsRNA. (*F*) Distance distribution from the four-pulse PELDOR measurements obtained by Tikhonov regularization. (*G*) Sequence of the seven-pulse-CP-PELDOR experiment. (*H*) Background corrected seven-pulse-CP-PELDOR time trace for a stacked singly labeled RNA. (*I*) Distance distribution from the seven-pulse-CP-PELDOR measurements obtained by Tikhonov regularization.

introducing an overhang of one nucleotide at both ends of the dsRNA.

RESULTS AND DISCUSSION

Our PELDOR measurements performed on singly labeled dsRNAs (Fig. 2) confirm that additional distances observed previously on doubly labeled dsRNAs (Piton et al. 2007; Romainczyk et al. 2011; Halbmair et al. 2016; Weinrich et al. 2017) are due to "end-to-end" stacking. PELDOR measurements with single-labeled dsRNAs exclusively show distances that result from intermolecular attraction between nucleic acids. This means that only stacked dsRNA molecules contribute to the modulation depth of the PELDOR signal after background division. As the stacking can occur at both ends of the strands, three different distances can be measured, as depicted in the cartoon in Figure 2C. Two distances can clearly be identified in the four-pulse PELDOR time traces (Fig. 2E,F). An additional higher distance peak (Fig. 2F, marked with a star) indicates the possible presence of a longer distance, but it is already beyond the distance range accessible with the maximum achievable four-pulse sequence time window of 7 μsec.

To be able to reliably observe the expected long distance seven-pulse-CP-PELDOR measurements were performed. With the Carr–Purcell (CP) pulse sequence (Fig. 2G), the length of the time traces can be significant extended to more than 17 μsec. Therefore, distances up to 10 nm can be measured. The seven-pulse-CP-PELDOR measurements confirm the shorter distances and show the expected additional distance at around 9 nm (Fig. 2H,I).

These distance distributions have been used for a simple geometrical interpretation of the orientations between two stacked dsRNA molecules, with each dsRNA molecule represented as a rigid cylinder. Assuming a rise per base pair of 0.28 nm, which is in full agreement with previous PELDOR measurements on doubly labeled dsRNA molecules (Halbmair et al. 2016), the mean values of all three measured intermolecular distances fit very well with a parallel end-to-end alignment of the dsRNA molecules (bend angle $\theta = 0$). To model the width of the experimental observed distance peaks, we used a Gaussian distribution of the bend angle θ:

$$P(\theta) = \frac{1}{\sqrt{2\pi}\sigma} e^{-\frac{\theta^2}{2\sigma^2}}. \quad (1)$$

Comparison of the experimental distance distribution widths for all three distance peaks resulted in a standard deviation σ of about 40°–50° for the kink angle distribution.

To inhibit the stacking, a nucleotide overhang was added to one end of one RNA strand during the solid phase synthesis. This prevents the possibility of a π–π interaction between the dsRNAs at one end; therefore, stacking can only lead to dimers with a single distinct distance as shown in the cartoon in Figure 3A. PELDOR measurements fully validated our expectations as they show only the high frequency oscillation corresponding to the short distance

Downloaded from rnajournal.cshlp.org on January 20, 2020 - Published by Cold Spring Harbor Laboratory Press

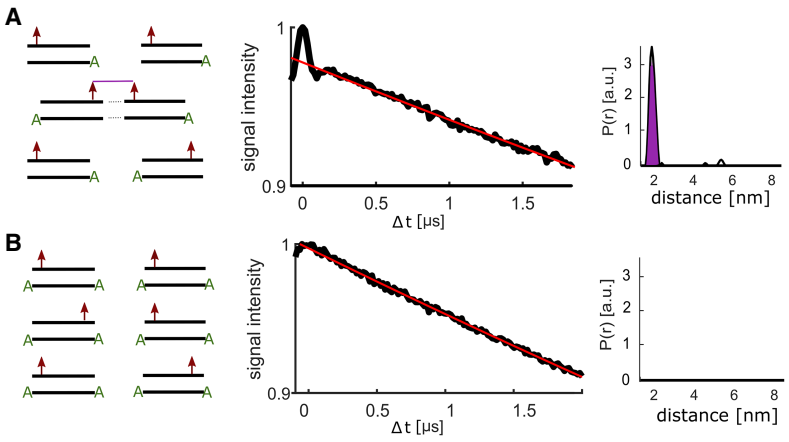

FIGURE 3. (*A*) dsRNA with a single nucleotide overhang at one end. (*B*) dsRNA with an overhang at both ends of the dsRNA. (*Left*) Schematic picture of stacking possibilities; (*middle*) raw four-pulse-PELDOR data; (*right*) Tikhonov derived distance distribution.

between the spin labels (Fig. 3A). In a second step, overhangs were added to both ends of one RNA strand. This led to the absence of any PELDOR oscillation, which indicates that there is no distinct distance and therefore a lack of stacking between the dsRNAs. The monotonous decay of the PELDOR signal in this case originates solely from the background signal arising from randomly distributed dsRNA molecules in the frozen solution sample (Fig. 3B).

Samples with different Na^+ concentrations were prepared to investigate the dependency of stacking on the concentration of monovalent counterions. The monovalent sodium concentration was varied between 50 and 800 mM, while keeping the dsRNA concentration constant at 200 μM. The overall shape of the PELDOR time traces remained constant (Supplemental Fig. S3A), but the modulation depth Δ systematically increased as a function of the salt concentration. The modulation depth Δ depends on the excitation efficiency λ of the nitroxide spin label by the microwave pump pulse and on the fraction of coupled spins. The excitation efficiency is given by the microwave field strength (given by the pulse length) and the spectral position (defined by the microwave frequency and magnetic field strength) and can be easily calibrated with nitroxide model compounds (Bode et al. 2007). For samples with a nucleotide overhang on only one end (Fig. 3A) only dimers and monomers can occur. In this case, the relation between the stacking probability *P* and the modulation depth Δ is especially simple:

$$\Delta = \lambda * P, \tag{2}$$

with the stacking probability *P* defined as

$$P = \frac{2(D)}{(M) + 2(D)} = \frac{2(D)}{(\mathrm{RNA})}. \tag{3}$$

Thus, the stacking probability *P* can be directly computed from the experimentally observed modulation depth Δ for the different salt concentrations (blue squares in Fig. 4A). For samples without any overhang higher oligomeric states can also occur. This leads to larger modulation depths for these samples (see Supplemental Fig. S3B). However, these samples yield the same stacking probability *P*, if statistics for the higher oligomeric states are taken into account (green diamonds in Fig. 4A, see Supplemental Material for details). The straight line in the diagram of Figure 4A serves only as an empirical correlation for the experimentally accessed salt concentration range. With Equation 3 and the thermodynamic definition of the dissociation constant K_d, the dissociation constant can be easily calculated for all salt concentrations from the derived stacking probabilities *P* and the known RNA concentration:

$$K_d = \frac{M^2}{D} = 2(RNA)\frac{(1-P)^2}{P}. \tag{4}$$

The dissociation constant K_d varies between 0.2 and 1.2 mM (Fig. 4B) for the experimentally accessed NaCl salt concentration, ranging from 50 to 300 mM. It should be mentioned that the dissociation constant itself is of course not a function of the RNA concentration; this factor is compensated by the intrinsic RNA concentration dependence of the stacking probability *P*, directly derived from the experiment (Fig. 4A).

In a second series of experiments, we measured the modulation depth as a function of the RNA concentration

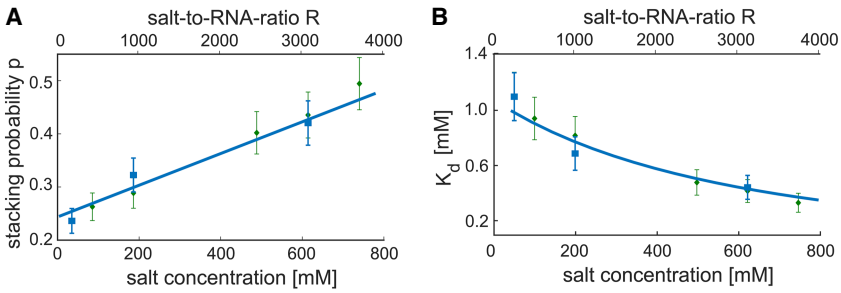

FIGURE 4. (*A*) Stacking probability of dsRNA in relation to the monovalent salt concentration of NaCl and to the salt-to-RNA ratio, for a RNA concentration of 200 μM. In blue for samples with one overhang and in green for samples without overhang but taking oligomers and multispin effects into account. The error was estimated to be 10%. (*B*) Dimerization constant K_d for the "end-to-end" stacking for different salt-to-RNA ratios. In blue for samples with one overhang and in green for samples without overhang but taking trimers and multispin effects into account. The error was estimated to be 10%.

Downloaded from rnajournal.cshlp.org on January 20, 2020 - Published by Cold Spring Harbor Laboratory Press

(ranging between 50 and 300 μM). These experiments were performed for two NaCl concentrations (200 and 500 mM). Surprisingly, no dependency of the stacking probability P on the RNA concentration itself was found (Fig. 5A).

Solving Equation 4 for the stacking probability P leads to the following expression:

$$P = 1 + C - \sqrt{C(C+2)}. \quad (5)$$

with

$$C = \frac{K_d}{4(RNA)}. \quad (6)$$

The second solution of the quadratic equation for P can be ignored because it would lead to values of $P > 1$. The stacking probability P calculated from Equation 5 for a NaCl concentration of 200 mM is shown in Figure 5B as dotted line. As expected, this curve shows increasing stacking probability for higher RNA concentrations, but it does not fit our experimentally determined stacking probabilities. On the other hand, our experimental findings can be successfully described by Equation 5 if we define the K_d values in Figure 4B not as a function of the absolute NaCl salt concentration but as a function of the ratio R between the NaCl salt and the RNA concentration. Whereas the overall NaCl concentration does not vary significantly for the experimentally accessed RNA concentration range between 50 and 300 μM, the ratio R does range from 4500 to 650. In this case, our experimental findings that P does not vary with RNA concentration can easily be rationalized by two counteracting effects. On the one hand, P increases with the RNA concentration (dotted line in Fig. 5B), but on the other hand P decreases because of the strongly reduced salt-to-RNA ratio R. The calculated P values taking K_d (R) explicitly into account are shown as a solid black line in Figure 5B and fits our experimental determined values within experimental error.

Our finding that the dissociation constant K_d does not depend on the absolute NaCl concentration, but rather on the ratio R between the absolute NaCl concentration and the overall RNA concentration is an interesting experimental observation. It is further supported by the fact that we find the expected dependence of P as a function of the RNA concentration with a constant K_d if we keep R constant (Supplemental Fig. S5) and vice versa that we get only a K_d value independent of the RNA concentration for one ratio R (Supplemental Fig. S6). Thus, all our experimental results are consistently described by Equation 5 and by taking K_d as a function of R.

Conclusions

In this work, "end-to-end" stacking of small dsRNA was studied by PELDOR spectroscopy. We synthesized 20mer dsRNAs containing one spin-label TPA per dsRNA molecule and performed four-pulse PELDOR and seven-pulse-CP-PELDOR measurements. The distinct dipolar modulations of the PELDOR time traces arise from the magnetic dipole–dipole interaction between two spin labels belonging to two stacked dsRNA molecules. The extracted distances confirm that the dsRNA stack "end-to-end" via π–π interaction of bases at the end of the strands. The kink angle distribution width of the stacked molecules could be estimated from the widths of the observed distance peaks.

The influence of monovalent NaCl salt concentration and of the dsRNA concentration itself on the stacking probability was investigated by the PELDOR signal modulation depth parameter Δ. Our measurements show that the stacking probability P and the dissociation constant K_d depend strongly on the overall NaCl to RNA concentration ratio R. Higher R ratios increase the stacking probability and decrease the dissociation constant. Varying the dsRNA concentration in a range between 50 and 300 μM for a constant sodium concentration therefore does not alter the stacking probability due to the simultaneous decrease of the salt-to-RNA-ratio. It should be stressed that the ratio R does not reflect on the local number of the salt ions per RNA molecule and that our experimental findings only have validity in NaCl and RNA concentration ranges tested in our experiments. An interpretation of our macroscopic findings in terms of the local ion atmosphere and screening around the dsRNA molecules (see, for example, Lipfert et al. 2014) is not part of this study. Nevertheless, we believe that our experimental

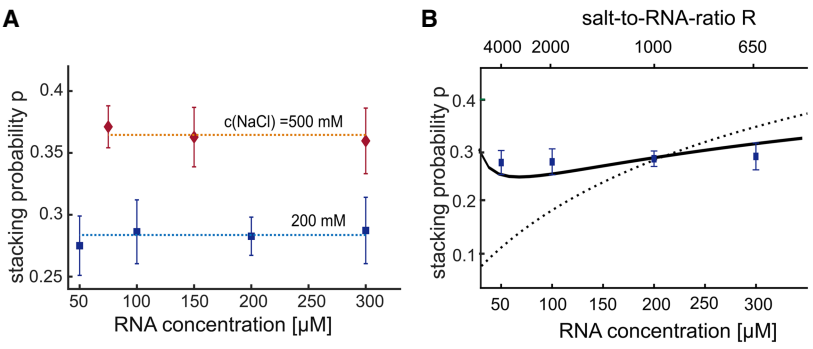

FIGURE 5. (*A*) Stacking probability of dsRNA in relation to the RNA concentration for 200 mM NaCl (blue) and 500 mM NaCl (orange). The error bars are statistical σ values of five measurements each. (*B*) Stacking probability of dsRNA in relation to the RNA concentration and the respective salt-to-RNA ratio for 200 mM NaCl concentration (blue data points). The dotted line indicates the expected behavior with a constant K_d and the black line with a K_d dependent on the salt-to-RNA ratio R.

Downloaded from rnajournal.cshlp.org on January 20, 2020 - Published by Cold Spring Harbor Laboratory Press

results and findings will be interesting for theoretical modeling of such local properties and optimization of MD simulations for these molecules. Similar experiments for dsRNA molecules in a cellular environment will be interesting and are on our agenda.

Further, we could prove by the PELDOR method that stacking of dsRNA molecules can be efficiently avoided by the addition of a nucleotide overhang at both ends of the dsRNA. For these experiments, an additional base was added during the solid-state synthesis of the individual strands at one end of the dsRNA or at both ends. While a base at one end still leads to a dimerization of dsRNA molecules, bases at both ends of the double strands fully inhibit stacking. This strategy is important for future investigations of the internal dynamics of dsRNA molecules by PELDOR spectroscopy currently in progress in our laboratory.

MATERIALS AND METHODS

Sample preparation

Spin-label TPA (2,2,5,5-Tetramethylpyrrolin-1-yloxyl-3-acetylene, structure depicted in Fig. 2B) was synthesized according to the literature (Schiemann et al. 2007; Azarkh et al. 2011). Oligonucleotide synthesis was performed using an Expedite Nucleic Acid Synthesis System from PerSeptive Biosystems and TBDMS-strategy amidites and standard protocols. The deprotection agent was dichloroacetic acid in dichloromethane, the coupling agent was 0.5 M ethylthiotetrazole, capping was performed using acetic anhydride in THF and *N*-methylimidazole in THF/pyridine, respectively. The oxidizing agent was iodine in THF/pyridine/H_2O. Since both the detritylation agent and oxidation agent are known to partially redox deactivate the spin label, the spin label was placed at the 5′-end of the oligonucleotide, and special care was taken to separate redox-deviated spin-labeled oligonucleotides. Oligonucleotide synthesis was stopped after the incorporation of the 5-iodouridine. Subsequently, TPA was coupled to the oligonucleotide by site-specific Sonogashira coupling to the 5-iodouracil base on solid support applying reported protocols (Schiemann et al. 2003; Grünewald et al. 2008). After the Sonogashira coupling, oligonucleotide synthesis was completed. For deprotection of phosphates and cleavage from solid support, cpg was removed from the column, suspended in 2 mL of a 3:1 mixture of 37% aq. ammonia/ethanol and incubated at 37°C for 18 h. Afterwards the supernatant was separated, the cpg material was washed two times with water and combined fractions were evaporated to dryness. TBDMS deprotection was performed by adding 300 µL of *N*-methylpyrrolidone/triethylamine (TEA)/TEA*3HF 6/3/4/v/v/v) and incubating at 65°C for 90 min. Precipitation with 1.2 mL butanol at −20°C and subsequent centrifugation yielded a pellet of crude oligonucleotide product.

The crude RNA was purified by AE-HPLC (A: water, B: 1 M LiCl; gradient: 0%–49% B for 30 min; flow 5 mL/min) on a JASCO LC-800. Further purification as well as concurrent desalting was typically accomplished by RP-HPLC (A: 1M TEAA buffer, B: water, C: acetonitrile; gradient: constant 10% A, 0%–45% C within 30 min; flow 4 mL/min) on a JASCO-2000 system including three times evaporation with water to remove buffering salt using a SpeedVac device.

Oligonucleotide concentrations were determined via UV spectrometry measurement on a nanodrop2000 (Thermo Scientific) applying the Lambert–Beer law. Extinction coefficients were determined by a nearest neighbor model according to the literature (Puglisi and Tinoco 1989; Gray et al. 1995). For that purpose, modified bases were considered correspondent to natural bases.

For all purification steps and resuspension, we used Milli-Q water that had been treated with 0.1% DEPC overnight and had been subsequently autoclaved.

The following oligonucleotides have been synthesized:

5′-GU XAG UCG CGC GCG CGC AUC-3′	(X = spin-labeled C)
3′-CA GUC AGC GCG CGC GCG UAG-5′	(no overhang)
3′-CA GUC AGC GCG CGC GCG UAG A-5′	(5′-overhang)
3′-ACA GUC AGC GCG CGC GCG UAG A-5′	(3′,5′-overhang)

EPR samples were prepared by resuspending the single strands in pure water, mixing the intended duplex of spin labeled oligonucleotide with counter strands with or without overhang and evaporation to dryness by SpeedVac. The oligonucleotide duplex was resuspended in buffer. Buffers used were phosphate buffer with different defined salt concentrations. Duplex concentration was set to 200 µM in a total volume of 30 µL if not otherwise stated. EPR samples contained 20% D8-glycol as cryoprotectant. For the determination of the intermolecular distances between the spin labels of dsRNA samples without overhang (Fig. 2) water was replaced by D_2O. This was necessary for increasing the transversal relaxation time T_2 of the spin label, allowing the recording of time traces with sufficient length. Before measurements, all samples were frozen in liquid nitrogen.

PELDOR methodology

The four-pulse PELDOR method was used to measure the distance between the spin labels and to measure the stacking probability of the dsRNA molecules. The pulse sequence is shown in Figure 1B. Pulses applied in PELDOR experiments have two distinct frequencies. The pump pulse frequency is typically set to be resonant with spins at the maximum of the nitroxide EPR spectra. This gives an optimal excitation efficiency λ, which depends on the applied microwave power and the chosen pulse length (for a π-pulse typically inversely related to the microwave power).

A refocused Hahn echo created by the probe pulses is used to monitor the magnetic dipole–dipole interaction between the nitroxide spins. The probe frequency is chosen 70 MHz below the pump frequency to avoid the pump and probe pulses affecting the same spins (typically called A and B spins affected by the probe and pump pulses, respectively). The flip of the B spin by the pump pulse shifts the Larmor frequency of the probed A spin, due to the dipolar spin–spin coupling. This reduces the intensity of the refocused Hahn echo, depending on the time Δt at which the pump pulse is applied. Recording the refocused Hahn echo intensity as a function of this time Δt results in the PELDOR time trace, which oscillates with the dipolar coupling frequency ω_{dd}.

PELDOR distances above 6 nm are challenging to measure, due to the limited observation time window of the four-pulse

Downloaded from rnajournal.cshlp.org on January 20, 2020 - Published by Cold Spring Harbor Laboratory Press

PELDOR sequence. We also used a seven-pulse-Carr-Purcell (CP)-PELDOR sequence here, recently developed in our laboratory, to extend the time window of the PELDOR measurement (Spindler et al. 2015). In the seven-pulse-CP-PELDOR experiment, three refocusing π pulses are applied at the probe frequency (as depicted in Fig. 2F), leading to a slower decay of the transversal magnetization of the observed A spin. A matching number of pump pulses on spin B have to be used to obtain the maximum evolution time window for observation of the dipolar coupling. Sech/tanh pulses were used as pump pulses to suppress artifacts arising from the nonuniform inversion efficiencies of rectangular pulses. Nevertheless, a parameter describing the nonquantitative inversion of the adiabatic inversion pulses has to be taken into account when analyzing the seven-pulse-CP-PELDOR signals. Artifact and background corrections were performed as described before (Spindler et al. 2015) and are shown in the Supplemental Material.

The PELDOR time traces were analyzed in terms of distances and modulation depth after background division, which was performed using the DeerAnalysis software (Jeschke et al. 2006).

Q-Band measurements

A Bruker Elexsys E580X/Q-band spectrometer equipped with an Oxford CF935 cryostat and a phase unlocked PELDOR frequency unit was used. Microwave pulses were amplified by a 10 W solid-state Q-band amplifier. Thirty-two nanoseconds (π/2 and π)-pulses were used for detection and a 16 nsec (π) pump pulse was used for the four-pulse PELDOR experiments. The delay between the first and second probe pulse was 132 nsec. The frequency of the pump pulse was fixed to the intensity maximum of the nitroxide powder spectrum to obtain optimal pumping efficiency. The probe frequency was chosen to be 70 MHz below this frequency.

In the seven-pulse-CP-PELDOR experiment, a sech/tanh pulse with a pulse length of 400 nsec and a bandwidth of 60 MHz was used as the pump pulse. All experiments were carried out at a temperature of 50 K.

SUPPLEMENTAL MATERIAL

Supplemental material is available for this article.

ACKNOWLEDGMENTS

We acknowledge financial support from the German Research Foundation (CRC902: Molecular Principles of RNA Based Regulation). The authors thank Professor S. Sigurdsson for fruitful discussions and Dr. P. Spindler and Dr. A. Collauto for their contribution to the seven-pulse-CP-PELDOR experiments.

Received July 17, 2018; accepted November 6, 2018.

REFERENCES

Allahyarov E, Gompper G, Löwen H. 2004. Attraction between DNA molecules mediated by multivalent ions. *Phys Rev E Stat Nonlin Soft Matter Phys* **69:** 041904. doi:10.1103/PhysRevE.69.041904

Azarkh M, Okle O, Eyring P, Dietrich DR, Drescher M. 2011. Evaluation of spin labels for in-cell EPR by analysis of nitroxide reduction in cell extract of *Xenopus laevis* oocytes. *J Magn Reson* **212:** 450–454. doi:10.1016/j.jmr.2011.07.014

Bode BE, Margraf D, Plackmeyer J, Dürner G, Prisner TF, Schiemann O. 2007. Counting the monomers in nanometer-sized oligomers by pulsed electron–electron double resonance. *J Am Chem Soc* **129:** 6736–6745. doi:10.1021/ja065787t

Brown RF, Andrews CT, Elcock AH. 2015. Stacking free energies of all DNA and RNA nucleoside pairs and dinucleoside-monophosphates computed using recently revised AMBER parameters and compared with experiment. *J Chem Theory Comput* **11:** 2315–2328. doi:10.1021/ct501170h

Endeward B, Butterwick J, MacKinnon R, Prisner TF. 2009. Pulsed electron–electron double-resonance determination of spin-label distances and orientations on the tetrameric potassium ion channel KcsA. *J Am Chem Soc* **42:** 15246–15250. doi:10.1021/ja904808n

Florián J, Šponer J, Warshel A. 1999. Thermodynamic parameters for stacking and hydrogen bonding of nucleic acid bases in aqueous solution: ab initio/Langevin dipoles study. *J Phys Chem* **103:** 884–892. doi:10.1021/jp983699s

Fonseca Guerra C, Bickelhaupt FM, Snijders JG, Baerends EJ. 1999. The nature of the hydrogen bond in DNA base pairs: the role of charge transfer and resonance assistance. *Chem Eur J* **5:** 3581–3594. doi:10.1002/(SICI)1521-3765(19991203)5:12<3581::AID-CHEM3581>3.0.CO;2-Y

Gellman SH, Haque TS, Newcomb LF. 1996. New evidence that the hydrophobic effect and dispersion are not major driving forces for nucleotide base stacking. *Biophys J* **71:** 3523–3526. doi:10.1016/S0006-3495(96)79547-4

Gray DM, Hung SH, Johnson KH. 1995. Absorption and circular dichroism spectroscopy of nucleic acid duplexes and triplexes. *Methods Enzymol* **246:** 19–34. doi:10.1016/0076-6879(95)46005-5

Grünewald C, Kwon T, Piton N, Förster U, Wachtveitl J, Engels JW. 2008. RNA as scaffold for pyrene excited complexes. *Bioorg Med Chem* **16:** 19–26. doi:10.1016/j.bmc.2007.04.058

Halbmair K, Seikowski J, Tkach I, Höbartner C, Sezer D, Bennati M. 2016. High-resolution measurement of long-range distances in RNA: pulse EPR spectroscopy with TEMPO-labeled nucleotides. *Chem Sci* **17:** 3172–3180. doi:10.1039/C5SC04631A

Häse F, Zacharias M. 2016. Free energy analysis and mechanism of base pair stacking in nicked DNA. *Nucleic Acids Res* **44:** 7100–7108.

Hunter CA, Sanders JKM. 1990. The nature of π–π interactions. *J Am Chem Soc* **112:** 5525–5534. doi:10.1021/ja00170a016

Jeschke G, Chechik V, Ionita P, Godt A, Zimmermann H, Banham J, Timmel CR, Hilger D, Jung H. 2006. DeerAnalysis2006—a comprehensive software package for analyzing pulsed ELDOR data. *Appl Magn Reson* **30:** 473–498. doi:10.1007/BF03166213

Kilchherr F, Wachauf C, Pelz B, Rief M, Zacharias M, Dietz H. 2016. Single-molecule dissection of stacking forces in DNA. *Science* **353:** aaf5508. doi:10.1126/science.aaf5508

Krstić I, Frolow O, Sezer D, Endeward B, Weigand JE, Suess B, Engels JW, Prisner TF. 2010. PELDOR spectroscopy reveals preorganization of the neomycin-responsive riboswitch tertiary structure. *J Am Chem Soc* **132:** 1454–1455. doi:10.1021/ja9077914

Lipfert J, Doniach S, Das R, Herschlag D. 2014. Understanding nucleic acid-ion interactions. *Annu Rev Biochem* **83:** 813–841. doi:10.1146/annurev-biochem-060409-092720

Maffeo C, Schöpflin R, Brutzer H, Stehr R, Aksimentiev A, Wedemann G, Seidel R. 2010. DNA–DNA interactions in tight supercoils are described by a small effective charge density. *Phys Rev Lett* **105:** 158101. doi:10.1103/PhysRevLett.105.158101

Martin RE, Pannier M, Diederich F, Gramlich V, Hubrich M, Spiess HW. 1998. Determination of end-to-end distances in a series of TEMPO

Downloaded from rnajournal.cshlp.org on January 20, 2020 - Published by Cold Spring Harbor Laboratory Press

diradicals of up to 2.8 nm length with a new four-pulse double electron electron resonance experiment. *Angew Chem Int Ed Engl* **37:** 2833–2837. doi:10.1002/(SICI)1521-3773(19981102)37:20<2833::AID-ANIE2833>3.0.CO;2-7

Mignon P, Loverix S, Steyaert J, Geerlings P. 2005. Influence of the π–π interaction on the hydrogen bonding capacity of stacked DNA/RNA bases. *Nucleic Acids Res* **33:** 1779–1789. doi:10.1093/nar/gki317

Milov AD, Ponomarev AB, Tsvetkov YD. 1984. Electron-electron double resonance in electron spin echo: model biradical systems and the sensitized photolysis of decalin. *Chem Phys Lett* **110:** 67–72. doi:10.1016/0009-2614(84)80148-7

Milov AD, Maryasov AG, Tsvetkov YD. 1998. Pulsed electron double resonance (PELDOR) and its applications in free-radicals research. *Appl Magn Reson* **15:** 107–143. doi:10.1007/BF03161886

Nakata M, Zanchetta G, Chapman BD, Jones CD, Cross JO, Pindak R, Bellini T, Clark NA. 2007. End-to-end stacking and liquid crystal condensation of 6 to 20 base pair DNA duplexes. *Science* **318:** 1276–1279. doi:10.1126/science.1143826

Oosawa F. 1968. Interaction between parallel rodlike macroions. *Biopolymers* **6:** 1633–1647. doi:10.1002/bip.1968.360061108

Pabit SA, Qiu X, Lamb JS, Li L, Meisburger SP, Pollack L. 2009. Both helix topology and counterion distribution contribute to the more effective charge screening in dsRNA compared with dsDNA. *Nucleic Acids Res* **37:** 3887–3896. doi:10.1093/nar/gkp257

Piton N, Mu Y, Stock G, Prisner TF, Schiemann O, Engels JW. 2007. Base-specific spin-labeling of RNA for structure determination. *Nucleic Acids Res* **35:** 3128–3143. doi:10.1093/nar/gkm169

Pollack L. 2011. SAXS studies of ion–nucleic acid interactions. *Annu Rev Biophys* **40:** 225–242. doi:10.1146/annurev-biophys-042910-155349

Puglisi J, Tinoco I. 1989. Absorbance melting curves of RNA. *Methods Enzymol* **180:** 304–325. doi:10.1016/0076-6879(89)80108-9

Qiu X, Kwok LW, Park HY, Lamb JS, Andresen K, Pollack L. 2006. Measuring inter-DNA potentials in solution. *Phys Rev Lett* **96:** 138101. doi:10.1103/PhysRevLett.96.138101

Qiu X, Andresen K, Kwok LW, Lamb JS, Park HY, Pollack L. 2007. Inter-DNA attraction mediated by divalent counterions. *Phys Rev Lett* **99:** 1–4.

Romainczyk O, Endeward B, Prisner TF, Engels JW. 2011. The RNA-DNA hybrid structure determined by EPR, CD and RNase H1. *Mol Biosyst* **7:** 1050–1052. doi:10.1039/c0mb00258e

Ryter JM, Schultz SC. 1998. Molecular basis of double-stranded RNA-protein interactions: structure of a dsRNA-binding domain complexed with dsRNA. *EMBO J* **17:** 7505–7513. doi:10.1093/emboj/17.24.7505

Schiemann O, Piton N, Mu Y, Stock G, Engels JW, Prisner TF. 2003. A PELDOR-based nanometer distance ruler for oligonucleotides. *J Am Chem Soc* **126:** 5722–5729. doi:10.1021/ja0393877

Schiemann O, Piton N, Plackmeyer J, Bode BE, Prisner TF, Engels JW. 2007. Spin labeling of oligonucleotides with the nitroxide TPA and use of PELDOR, a pulse EPR method, to measure intramolecular distances. *Nat Protoc* **2:** 904–923. doi:10.1038/nprot.2007.97

Spaltenstein A, Robinson BH, Hopkins PB. 1989. Sequence- and structure-dependent DNA base dynamics: synthesis, structure, and dynamics of site, and sequence specifically spin-labeled DNA. *Biochemistry* **28:** 9484–9495. doi:10.1021/bi00450a036

Spindler PE, Waclawska I, Endeward B, Plackmeyer J, Ziegler C, Prisner TF. 2015. Carr–Purcell pulsed electron double resonance with shaped inversion pulses. *J Phys Chem Lett* **6:** 4331–4335. doi:10.1021/acs.jpclett.5b01933

Šponer J, Bussi G, Krepl M, Banáš P, Bottaro S, Cunha RA, Gil-Ley A, Pinamonti G, Poblete S, Jurečka P, et al. 2018. RNA structural dynamics as captured by molecular simulations: a comprehensive overview. *Chem Rev* **118:** 4177–4338. doi:10.1021/acs.chemrev.7b00427

Sturtevant JM, Rice SA, Geiduschek EP. 1958. The stability of the helical deoxyribonucleic acid (DNA) molecule in solution. *Disc Faraday Soc* **25:** 138–149. doi:10.1039/df9582500138

van de Waal BW. 1986. Computed structure of small benzene cluster. *Chem Phys Lett* **123:** 69–72. doi:10.1016/0009-2614(86)87017-8

Weinrich T, Gränz M, Grünewald C, Prisner TF, Göbel MW. 2017. Synthesis of a cytidine phosphoramidite with protected nitroxide spin label for EPR experiments with RNA. *Eur J Org Chem* **2017:** 491–496. doi:10.1002/ejoc.201601174

Wong GC, Pollack L. 2010. Electrostatics of strongly charged biological polymers: ion-mediated interactions and self-organization in nucleic acids and proteins. *Annu Rev Phys Chem* **61:** 171–189. doi:10.1146/annurev.physchem.58.032806.104436

Downloaded from rnajournal.cshlp.org on January 20, 2020 - Published by Cold Spring Harbor Laboratory Press

"End-to-end" stacking of small dsRNA

Nicole Erlenbach, Christian Grünewald, Bisera Krstic, et al.

RNA 2019 25: 239-246 originally published online November 7, 2018
Access the most recent version at doi:10.1261/rna.068130.118

Supplemental Material http://rnajournal.cshlp.org/content/suppl/2018/11/07/rna.068130.118.DC1

References This article cites 41 articles, 3 of which can be accessed free at:
http://rnajournal.cshlp.org/content/25/2/239.full.html#ref-list-1

Creative Commons License This article is distributed exclusively by the *RNA* Society for the first 12 months after the full-issue publication date (see http://rnajournal.cshlp.org/site/misc/terms.xhtml). After 12 months, it is available under a Creative Commons License (Attribution-NonCommercial 4.0 International), as described at http://creativecommons.org/licenses/by-nc/4.0/.

Email Alerting Service Receive free email alerts when new articles cite this article - sign up in the box at the top right corner of the article or **click here.**

To subscribe to *RNA* go to:
http://rnajournal.cshlp.org/subscriptions

© 2019 Erlenbach et al.; Published by Cold Spring Harbor Laboratory Press for the RNA Society